Resonant ion-pair formation and dissociative recombination in electron collisions with ground-state HF^+ ions

N. Djurić* and G. H. Dunn
JILA, University of Colorado and National Institute of Standards and Technology, Boulder, Colorado 80309-0440

A. Al-Khalili, A. M. Derkatch, A. Neau, S. Rosén, W. Shi, L. Vikor, W. Zong, and M. Larsson
Department of Physics, Stockholm University, Box 6730, S-113 85 Stockholm, Sweden

A. Le Padellec
LCAR UMR 5589 Universite Paul Sabatier-Tolouse III 118, route de Narbonne, Bâtiment III R1, b4, 31062 Toulouse Cedex 4, France

H. Danared and M. af Ugglas
Manne Siegbahn Laboratory, Stockholm University, S-104 05 Stockholm, Sweden
(Received 22 March 2001; published 13 July 2001)

Rate coefficients and absolute cross sections for center-of-mass energies between 0.0001 and 1 eV are reported for both resonant ion-pair formation and dissociative recombination in electron collisions with HF^+ ions. The heavy-ion storage ring CRYRING in Stockholm was used for these measurements. Notable is the fact that the dissociative recombination cross section is substantially smaller than that for most diatomic molecular ions. The recombination seems to have an underlying E^{-1} energy dependence characteristic of the *direct* process in dissociative recombination, but both cross sections show structure, which may be attributed to contributions from different *indirect* processes. The cross sections have no observable energy thresholds. The ratio of the cross section for resonant ion-pair formation to that for dissociative recombination is about 0.25 at 10^{-3} eV, with the ratio depending on the interaction energy, so the competition of the ion-pair process is much stronger than for other ions so far studied. The HF^+ ion is unique in the fact that the electron affinity of F, the binding energy of HF^+, and energy of the atom pair $[H(n=2)+F(^2P_{3/2})]$ are the same within the rotational-energy spread of the HF^+ target. The resonant ion-pair formation process, $e+HF^+ \rightarrow H^+ + F^-$, has some similarities to the photon process, $h\nu + HF \rightarrow H^+ + F^-$, and we discuss comparisons. We deduce thermal rate coefficients from our measurements and discuss them in the context of rate coefficients for other diatomic ions available in the literature.

DOI: 10.1103/PhysRevA.64.022713 PACS number(s): 34.80.Gs, 34.80.Ht, 34.80.Kw, 34.80.Lx

I. INTRODUCTION

A. General

In this paper, we discuss the experimental study of two dissociative processes resulting from electron impact on vibrationally relaxed HF^+ ions. We consider processes wherein an electron is resonantly captured by the ion, losing its kinetic energy to either electronic or vibrational excitation of the resulting neutral molecule. Dissociation of the compound state can occur rapidly and compete favorably with reionization (autoionization), and depending on what dissociative channels are followed, one may end up with neutral fragments [dissociative recombination (DR)] or ion-pair fragments [resonant ion-pair formation (RIP)] with the excess energy appearing as kinetic energy of the fragments in each case. A review paper on the dissociative recombination process with ion-storage rings was recently published [1].

For HF^+ targets the process resulting from electronic excitation and capture (often referred to as the *direct* process) may be represented as

$$e + HF^+(v=0) \rightarrow HF^{**} \rightarrow H + F + E_{DR}^{\mathrm{kin}}, \tag{1a}$$

$$e + HF^+(v=0) \rightarrow HF^{**} \rightarrow H^+ + F^- + E_{RIP}^{\mathrm{kin}}, \tag{1b}$$

where E^{kin} is the kinetic-energy release. Not shown in Eq. (1) are possible internal excitation of the fragments and the existence of another RIP channel, $H^- + F^+$, which is not observed due to apparatus constraints. The process resulting from vibrational excitation and capture (often referred to as the *indirect* process) can be represented as

$$e + HF^+(v=0) \rightarrow HF_{nv}^{Ryd} \rightarrow HF^{**} \rightarrow H + F + E_{\mathrm{DR}}^{\mathrm{kin}}, \tag{2a}$$

$$e + HF^+(v=0) \rightarrow HF_{nv}^{Ryd} \rightarrow HF^{**} \rightarrow H^+ + F^- + E_{\mathrm{RIP}}^{\mathrm{kin}}. \tag{2b}$$

Here the electron is resonantly captured into a neutral Rydberg state HF_{nv}^{Ryd} that converges to a bound ionic state that subsequently predissociates through the dissociative state, HF**. In each case, DR and RIP involve stabilization of the same compound state HF**, and one may expect some similarities between these two cross sections.

In fact, the indirect process may also take place by a combination of *both* electronic *and* vibrational excitation as the electron is captured. Typically, when this is the case, one

*Corresponding author.
Email address: nada@jilau1.colorado.edu

is referring to a ''core-excited'' state of the molecular ion. This has been invoked to describe DR and some observed structure for a number of ions [2–5].

DR is a key collision process in the physics of plasmas where molecular ions are present. It can alter the state of ionization of the medium and lead to the formation of products that are physically and chemically different from the primary plasma constituents. Studies of dissociative collisions of electrons with molecular ions have been dominated for decades by the examination of DR [1,6].

On the other hand, much less attention has been paid to the RIP process [7]. Only a few molecular ions have been previously studied: experimentally H_2^+ [8] and H_3^+ [9,10], and theoretically H_2^+ [11] and HeH^+ [12]. A recent paper [13] described the experimental study of RIP for cold diatomic molecular ions and reported partial results for HD^+, OH^+, and HF^+. A subsequent paper [14] described the results for HD^+ and OH^+ in more detail and presented some theoretical calculations for HD^+. This paper discusses the experiment and results for HF^+ in more detail.

The importance of studying DR and RIP for HF^+ is based partly in some unique physics characteristic of this molecule, and this will be discussed later. It is also founded in the abundant occurrence of HF in nature and in industry. For example, HF has been discovered to be present in various interstellar clouds along with some 118 other molecules [15]. The modeling of the clouds' compositions involves knowledge of the reactions we study here. The molecule has also been found [16] in planetary atmospheres as well. Industrial production of HF has increased remarkably in recent years [17] due to its use in the continually developing electronic and photochemical industries. The behavior of the ion in etching plasmas is of serious interest to the electronics industry [18], and chemical lasers involving HF are of renewed interest [19] in defense issues.

As noted above, we briefly reported DR and RIP results for HF^+ [13]; but other than this, neither experimental results nor theoretical calculations have so far been carried out for DR or RIP of HF^+. Thus, we present here the first measurements of the rate coefficients and deduced cross sections for this member of the hydrogen-halide family.

B. The molecular system

The electronic states of HF^+ are illustrated in Fig. 1(a). Two potential-energy curves for HF^+, the ground $X\,^2\Pi$ and the excited $A\,^2\Sigma^+$ state [20], are effectively isolated from the manifold of other states in the HF^+ molecule [not shown in Fig. 1(a)] that are almost 4 eV above. The two lowest states of HF^+, $X\,^2\Pi_{3/2,1/2}$ and $A\,^2\Sigma^+$, both correlate to the common asymptotic limit $H^+ + F(^2P)$, a fact that makes HF^+ unique among the halogen-halide series, as well as among many diatomic molecules. This is due to the much higher ionization potential [21] of the F atom (17.423 eV) compared to that of the H atom (13.598 eV). The $A\,^2\Sigma^+$ state is found to correlate to the $H^+ + F(^2P_{1/2})$ limit, whereas both spin-orbit components of the $X\,^2\Pi$-state correlate to the $H^+ + F(^2P_{3/2})$ limit that lies 50 meV lower in energy. The spin-orbit splitting of the ground $X\,^2\Pi_{3/2,1/2}$ state is on the order of

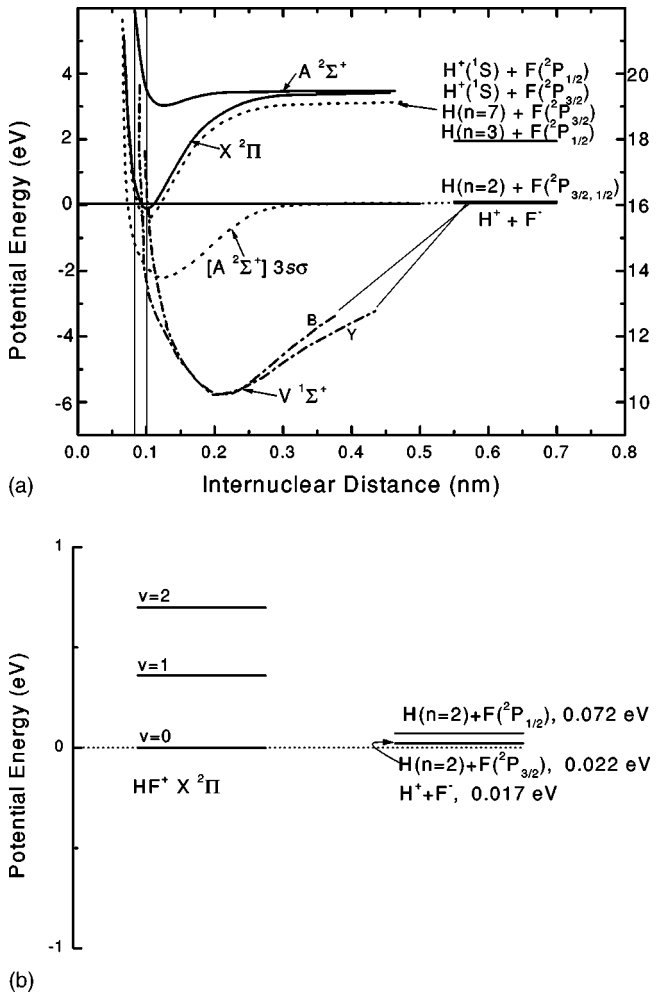

FIG. 1. (a) Potential-energy curves of the relevant HF^+ states. Bold lines: the ground $X\,^2\Pi$ and the first excited $A\,^2\Sigma^+$ state, taken from Ref. [20]. Two possible potential-energy curves for the $V\,^1\Sigma^+$ state (B and Y, both drawn as dot-dashed lines) are included [22,23]. Potential-energy curve of the core excited $3s\sigma$ Rydberg state converging to the $A\,^2\Sigma^+$ is drawn as a dotted line and is taken from Ref. [20]. The Rydberg state ($n=7$, also drawn as a dotted line) converging to the ground $X\,^2\Pi$ ionic state is calculated by subtracting $13.6/n^2$ from the curve of the $X\,^2\Pi$ state. The Frank-Condon region for excitation from the ground state of HF is shown by the double vertical lines. (b) Expanded view showing the essential coincidence in energy of (1) the ground state of HF^+, (2) the asymptotic limit giving $H(n=2)+F(^2P_{3/2})$, and (3) the asymptotic limit giving $H^+ + F^-$, i.e., the ion pair. The $X\,^2\Pi_{1/2}$ state (not shown) lies about 30 meV above the $X\,^2\Pi_{3/2}$ level.

30 meV. The potential-energy curve for the $V\,^1\Sigma^+$ ion-pair state with $H^+ + F^-$ dissociation limit is especially important for both the DR and RIP processes. Unfortunately, there are discrepancies in the literature concerning the potential-energy curves for the $V\,^1\Sigma^+$ state, and two possible potential-energy curves [22,23] for this state are included in Fig. 1(a). Potential-energy curves for the first Rydberg state, the $3s\sigma$ state, converging to the $A\,^2\Sigma^+$ state, with $H(n=2)+F(^2P_{1/2})$ dissociation limit is taken from Yencha *et al.* [23] and is included in Fig. 1(a). Only one approximate curve that converges to the $X\,^2\Pi$ ground-ion state is shown,

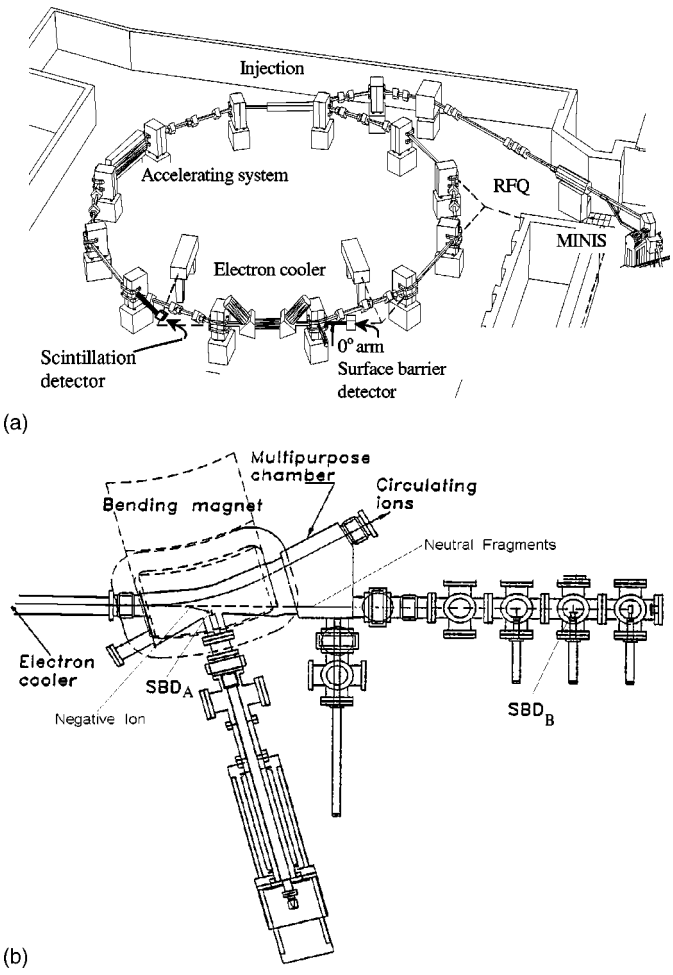

FIG. 2. (a) The CRYRING facilities in Stockholm, and (b) view of the CRYRING dipole magnet chamber with surface barrier detectors for negative ions (SBD_A inside the dipole chamber) and for neutral fragments (SBD_B in the zero arm).

and that is one that asymptotically gives hydrogen in the $n=7$ level. Note that Fig. 1(a) does not present the separate spin-orbit components of the $X\,^2\Pi_{3/2,1/2}$ ground state; though not shown, the presence of both components of the Rydberg series that lie just below the HF^+ ground state certainly will affect the *indirect* dissociation process.

Figure 1(b) illustrates in more detail the essential coincidence in energy of (1) the ground state of HF^+, (2) the asymptotic limit giving $H(n=2)+F(^2P_{3/2})$, and (3) the asymptotic limit giving $H^+ + F^-$, i.e., the ion pair. As pointed out earlier, this coincidence of energies is also a unique quality of the system under study.

II. EXPERIMENTAL METHOD

A. Overview

In these studies we used a combination of the well-known merged-beams and ion-storage-ring technologies implemented at the heavy-ion storage ring CRYRING in Stockholm. Schematic representations are shown in Figs. 2(a) and 2(b). More complete discussions of the experimental method may be found elsewhere [24]. We limit ourselves here to specifics of this experiment.

With reference to Fig. 2(a), ions are produced in a hot-filament discharge source (MINIS) containing a mixture of CF_4 and H_2 gases. After extraction from the source, the ions are mass selected, accelerated, and injected into the storage ring. In the ring the HF^+ ions are further accelerated to $E_i = 4.8$ MeV. A typical circulating current of HF^+ in our experiment was 130 nA. As the ions circulate in the ring, infrared active ions decay to their vibrational ground state before data taking is started. Relaxation is insured provided the radiative lifetimes are short compared to the storage time before data taking begins. According to theoretical calculations for the lifetime of excited vibrational levels of the $X\,^2\Pi$ state [25] of HF^+ the radiative lifetime for the vibrational transition from $v=1$ to $v=0$ is 1.6 ms. The lifetime for the electronic radiative decay of the excited $A\,^2\Sigma^+$ is of the order of 20 μs [25]. After looking at all available lifetime data for the ion, it is expected that full relaxation of excited vibrational and electronic states produced in the ion source will occur in much less than one second, so that by 6 s after injection when data recording is started, the ions are electronically and vibrationally relaxed.

At each turn, in one of the straight sections of the ring known as an ''electron cooler'' [26], the ion beam is merged with a velocity-matched electron beam, which for our 4.8 MeV HF^+ was a 3.3 mA beam of 142 eV electrons with 40 mm diameter. The electron-velocity distribution in the ion rest frame is described by a flattened Maxwellian distribution function [27] characterized by different transverse ($kT_\perp = 1$ meV) and longitudinal ($kT_\parallel = 0.1$ meV) temperatures. The purpose of the cooler is twofold: first, the electron beam is used to translationally cool the stored-ion beam; second, the electron beam serves as a target in the electron-ion collision experiments. The extent of the translational cooling with attendant reduction of the ion-beam size, depends on the charge-to-mass ratio of the ions. In this experiment the ions are relatively heavy ($M=20$), and cooling is not very efficient. Nevertheless, the velocity spread ($\Delta v/v = 10^{-3}$) of a noncooled ion beam contributes only about 0.4 meV at an interaction energy of 1.0 meV and contributes only 0.025 eV at 1-eV interaction energy; so decent energy resolution is attainable here even without full cooling. Thus, the distribution of relative velocities between the ions and electrons is dominated by the electron-velocity distribution.

On the basis of previous experiments and the energy-resolution observed therein, we can expect an energy resolution of about 1–2 meV at 1-meV interaction energy and about 12-meV resolution at 100-meV interaction energy for a reasonably cooled, centered, and aligned ion beam. An uncertainty in this arises due to space-charge effects in the electron beam. The kinetic energy of the electrons in the beam is not uniform over the electron-beam cross section because of the electron space charge. This radial dependence of electron energy has important experimental consequences. First, an ion traveling through the electron beam at a finite angle with respect to the electron-beam axis experiences a broader energy distribution than an ion traveling parallel to that axis. Second, due to the finite ion-beam diameter, ions with different positions along the radius interact with electrons of different energies. If the ion beam were to traverse the entire

electron beam from center to edge by being tilted, the energy resolution could be degraded by about 0.4 eV in the center-of-mass (c.m.) energy frame. However, with the cooling available and careful centering of the ion beam, we are confident that this effect has been minimized. As will be seen in the data, features at about 100 meV suggest an energy resolution of no worse than 20 meV at that energy.

Following the electron cooler, the parent ions and product ions are bent by a dipole magnet, while the neutral products follow a straight line and hit a 40-mm diameter, energy-sensitive surface-barrier detector (SBD_B) located 4.5 m downstream. A 27-mm diameter SBD_A, mounted on a linear-motion feedthrough, is placed inside the dipole chamber and used to detect heavy negative-ion fragments, i.e., F^- [see Fig. 2(b)]. These detectors have 100% detection efficiency for the ion-beam energies used here.

Potentials between the cathode and adjoining electrodes are constant throughout the experiment, and the entire gun is raised and lowered in potential as energies are scanned. Thus, the electron current is constant throughout the experiment, and the electron-collector current is actually measured only once during the experiment.

The absolute ion current is, in principle, measured using a coil in which a current is induced as the ion beam passes through it. In practice this is difficult when using ions heavier than a few amu unless the ion currents are large. Hence it is not practical to measure the ion current directly with this method throughout the entire data cycle. Instead, an auxiliary ion-current measuring device is implemented. This consists of a scintillation detector at the end of one of the straight sections as shown in Fig. 2(a). Neutrals formed by ion collisions with background gas hit this detector and give count rates proportional to the gas density and the ion current. The count rate R_s here is related carefully to the ion current I_i when it is large enough to be measured absolutely with the coil method. Gas density in the system is constant and monitored, so the device is linear with ion current provided the count rates are within the limits set by dead times of the counting system. Thus, one has a secondary calibrated ion-current meter such that $I_i = C_s R_s$, with C_s being a constant. This can be used to measure ion current over the large dynamic range of ion currents encountered during the measurements.

B. Data protocol

After each ion injection, a few seconds are allowed for vibrational and electronic de-excitation of the ions, during which time the ions are accelerated to full beam energy. After full acceleration, the ions are cooled for 6 s using electrons with the same average velocity as the ions. The electron-cooling energy is $E_{cool} = E_i m_e / m_i$, where E_i is the energy of the ions, and m_e and m_i are the electron and ion masses, respectively. Once the beams are aligned, and the ion beam relaxed and cooled, the interactions take place over a range of relative velocities achieved by detuning the electron-gun-cathode voltage.

Within 10 ms, the electron velocity is detuned, and at that time the energy scan is begun. The center-of-mass energy is given by $E_{cm} = (\sqrt{E_d} - \sqrt{E_{cool}})^2$, where E_d is the average detuned laboratory electron energy, and E_{cool} is the laboratory electron energy when cooling occurs. As shown in Fig. 3, the cathode voltage first rises, making the electrons *faster* than the ions (the voltage is set to correspond to a c.m. energy of 1 eV), then is ramped down in about 2 s through the cooling voltage and on to its minimum (corresponding to a c.m. energy of 1 eV, electrons being *slower* than the ions) and then back, in 10 ms, to the cooling voltage for an additional 2 s. Next, the voltage ramp is changed for the DR measurements: the cathode voltage is initially set to a value corresponding to 2-eV c.m. energy, with electrons *faster* than the ions. Then within 2 s the voltage is ramped through the cooling value to a value that corresponds to 0.2-eV c.m. with electrons *slower* than the ions, and then the gun is switched back to the cooling voltage. The data cycle is finally completed by holding the electron beam at its cooling energy for 2 s more. For each ion injection cycle (lasting 14 s), two RIP and two DR spectra are obtained, with electrons being *faster* and *slower* respectively than the ions, thus providing a consistency check on the data including the availability of obtaining (finding) the zero relative energy.

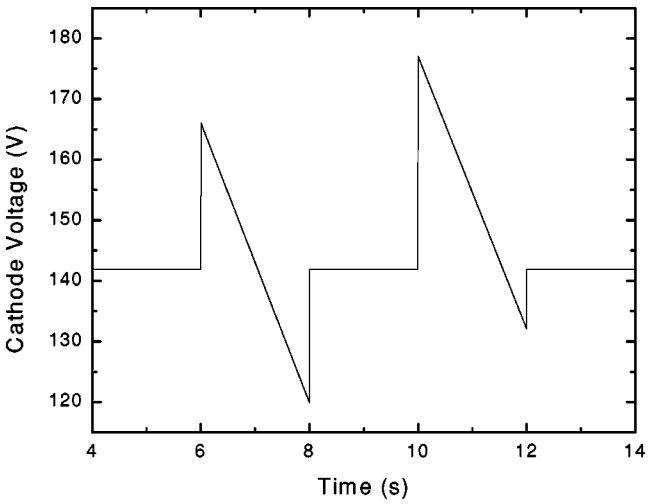

FIG. 3. Schematic view of the cathode voltage scan as a function of time during one injection cycle.

Counts from the SBD's are registered in a multiscaler device with a fixed dwell time for each scaler so that as interaction energy is varied in time as shown in Fig. 3, there is a defined correspondence between scaler (channel) number and interaction energy. Since pulse heights in the SBD's are proportional to the energies of the impacting particles, discriminator levels are set so that only the particles of interest to either RIP or DR are counted. At the same time, ion current is recorded in a fashion (via scintillator) that the known current can be used in connection with the measured counts in a given scaler.

C. Data analysis

The rate of production of scattering events S between electrons of density N_e and ions of density N_i colliding at relative velocity v_r, where the cross section is σ, is given by [7]

$$S=\int N_e N_i v_r \sigma dV$$

$$=\frac{I_i I_e \sigma v_r}{q e^2 v_i v_e}\frac{\int \Gamma_i \Gamma_e dV}{\int \Gamma_i dA_i \int \Gamma_e dA_e}=\frac{I_i I_e \sigma v_r}{e^2 v_i v_e}\frac{L}{A_e}, \quad (3)$$

where use has been made of the fact that v_r and σ are constant throughout the collision volume V, that $q=1$ for these molecular ions, and the fact that the ion beam of cross sectional area A_i and diameter between 1 and 3 mm is well contained within the 40-mm diameter quite uniform electron beam of cross sectional area A_e and length L. Then, making use of the relationship that the rate coefficient is just $v_r\sigma=\alpha$, and solving for α, we have

$$\alpha=(Se^2 v_e v_i A_e)/LI_e I_i=(Se^2 v_e v_i A_e)/LI_e(C_s R_s), \quad (4)$$

where the form of this equation used depends upon how I_i is determined.

Thus, because of the electron-velocity spread, we do not measure cross sections at very low energies. Instead, we measure the rate coefficients, α, that are the velocity-weighted cross sections averaged over the velocity distribution $f(v)$ of the electrons for a relative velocity v:

$$\alpha=\langle \sigma(v) v\rangle=\int v\sigma(v) f(v) d^3 v. \quad (5)$$

We have assumed the velocity distribution of electrons is known and have used a Fourier transform based procedure described in detail elsewhere [28] to obtain the cross section at the lowest energies and have simply divided the rate coefficient by velocity at energies above 0.01 eV to get the cross sections.

Regrettably, in an oversight, the ion current in terms of R_s was not recorded during the scan period when measuring DR (see Fig. 3). Thus, the exponential decay of the ion current, which was well-established during the RIP measurements, was assumed to continue through this period of time, and the extrapolated current was used for analysis of the DR data. Because of the smooth behavior of the ion current during the RIP measurements, and based on past experience with ion-beam decay, we judge that this procedure is justified, but it adds an additional uncertainty to the DR results, discussed later.

To obtain the signal count rates, S, to be used in Eq. (4), it was necessary to subtract background count rates to the detector. The ''backgrounds'' were defined to be the apparent ''signal'' level at an energy where the signal was not changing (flat) with energy at a level determined by statistical precision. For RIP, these background rates were down to about 1 s^{-1} compared to the level of signal of several thousand per second at the lowest energy (0.1% at 0.001 eV to 40% at 0.9 eV). The ''defined'' background rates similarly determined were more substantial in the case of DR, where the ion-residual gas background cross section was larger, and were about 380 s^{-1} compared to a few thousand per second at the lowest energy (12% at the lowest energy to 90% at 0.9 eV).

A number of corrections routinely applied to the data in the ring are applied here. First, we correct the c.m. energy, for the electron space charge [29]. Second, we correct for the so-called toroidal effect. This is necessary, since the electrons are merged with the ions using a toroidal magnet, and over some short distance the angle between the velocities is not zero, thus causing higher energies over this merging path. To correct for this effect, we used an iterative procedure [30]. Finally, when the velocity of the electrons is tuned away from the ion velocity, i.e., from cooling, the ions are dragged towards the electrons resulting in a change in the c.m. energy. This effect is strong for low c.m. energies and for light molecular ions, but is not appreciable for molecular ions as heavy as used here. Nevertheless, the c.m. energy was corrected for this effect by applying a procedure described by DeWitt *et al.* [31].

The estimated absolute uncertainty in the RIP measurements at the lowest energies is about 20% at the 1σ level. This is dominated by the uncertainty in the ion-beam current (15%), the electron density (5%), and the effective length of the electron cooler (10%). To obtain the total uncertainty, one must, of course, include the statistical uncertainty that varies from 1% at 0.001 eV to 90% at 0.9 eV. For the DR measurements, as noted earlier, the uncertainty in the ion current is estimated to be 30%, while the uncertainties in the electron density and effective length remain the same. Thus, the absolute uncertainty in the DR measurements is estimated to be 32% at the 1σ level, and the statistical uncertainty ranges between 3% at 0.001 eV to 70% at 0.9 eV. Because of the high uncertainty in the DR spectra at the highest energies, data above 1 eV are not presented even though they were recorded.

III. RESULTS

A. General

Absolute rate coefficients for DR and RIP of HF^+ over the c.m. energy range 0.0001 to 1 eV are presented in Fig. 4, and the corresponding cross sections deduced as described earlier are shown in Fig. 5. The ratio of the cross sections (RIP/DR) is shown in the lower part of the Figure, with the scale on the right. Certain features immediately stand out as one examines these figures.

(1) The DR rate coefficients (and corresponding cross sections) are significantly smaller than one normally encounters for diatomic ions when there is a crossing of the repulsive portion of a neutral curve near the ground-ionic-state potential minimum as is the case here.

(2) The general trend of both cross sections with energy is roughly E^{-1} up to 0.03 eV, but there are structural features associated with both. Beyond 0.03 eV, ignoring the features, the general trend of the DR cross section continues roughly as E^{-1} up to 1 eV, while the RIP cross section assumes a much steeper decline with energy.

(3) At low energy up to 0.1 eV, the RIP process competes strongly with DR, with the cross section ratio being about

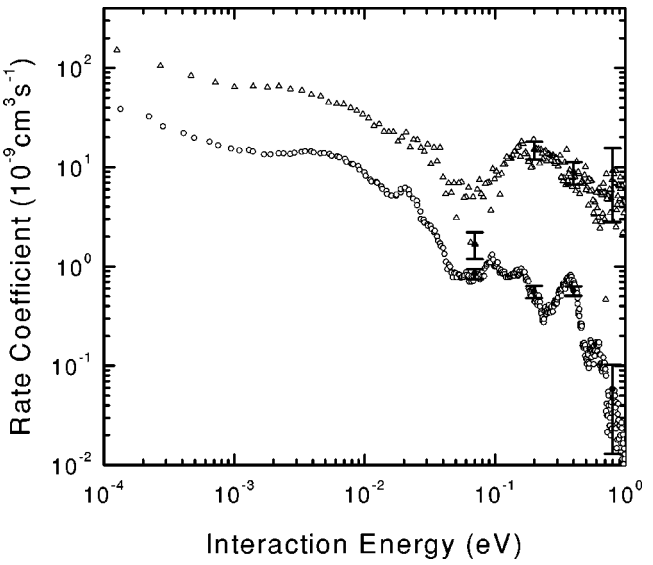

FIG. 4. Absolute rate coefficient for HF^+ as a function of interaction energy: (△) DR and (○) RIP. Statistical uncertainties are shown for selected points. At 0.001 eV the uncertainties are smaller than the points. For DR they are drawn: 30% at 0.07 eV; 20% at 0.2 eV; 25% at 0.4 eV; and 70% at 0.8 eV. For RIP they are 12%, 14%, 11%, and 80% at the same selected energies.

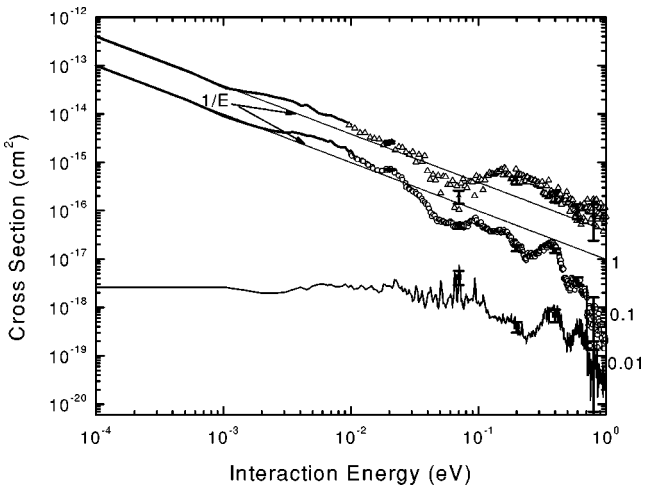

FIG. 5. Absolute cross sections for HF^+ as a function of interaction energy. Solid curves show the cross sections (DR and RIP) as derived from the measured rate coefficients using a deconvolution procedure described in [28]. Points show the cross sections derived by dividing the measured rate coefficient by the relative velocity (for $E \geqslant 0.01$ eV); (△) DR and (○) RIP. The statistical uncertainties are shown at 0.8, 0.6, 0.4, 0.2, and 0.07 eV. Curves decaying as E^{-1} are shown to help demonstrate that dependence of the measurements. The ratio of the cross sections (RIP/DR) is shown in the lower part of the figure, with the scale on the right. Clearly, the rapid fluctuations in the ratio curve are due primarily to statistical uncertainties in the measured cross sections. The statistical uncertainties, taken as the square root of the quadrature sum of the individual statistical uncertainties are shown at 0.8, 0.4, 0.2, and 0.07 eV.

0.3. As energy increases beyond this, the ratio gets much smaller. Given the potential curves and asymptotic energies involved, this strong competition was somewhat expected.

(4) There is no observed positive-energy threshold for the rates/cross sections for either of the processes. This is consistent with the potential curves and energies of Figs. 1(a) and 1(b), the thermal rotational energies of the ions, and the energy resolution of the experiment.

(5) Certain of the structural features are common to both DR and RIP, while fewer features show up in the DR curves. This is due in large part to the much poorer statistical precision of the DR data. The most obvious commonalities are the broad ''hump'' in the cross section between about 0.002 eV and 0.02 eV and the very steep decline in the cross sections at about 0.04 eV leading to minima in the two cross sections at around 0.07 eV.

1. Dissociative recombination

The general E^{-1} trend of the DR cross section and recognition that the $V\,^1\Sigma^+$ state crosses through the $X\,^2\Pi$ state between the classical turning points of the $v=0$ vibrational level lead to the normal hypothesis that direct capture and stabilization through the $V\,^1\Sigma^+$ state accounts for most of the recombination. However, the small size of the cross section and the presence of structure lead to the conjecture that one or more *indirect* processes are operative and interfering with the direct process.

A striking structural feature common to both the DR and RIP curves of Figs. 4 and 5 is the steep decline of the cross section with energy starting about 0.04 eV culminating in a minimum about 0.07 eV. The observations of strong autoionization peaks at corresponding energies in photoionization experiments [22,32] leads us to adopt the hypothesis that this drop in the two cross sections is due to strong autoionization. We can thereby also suggest the assignment given by the authors of the photon work and say that tentatively the increased autoionization is associated with a Rydberg state of the $^2\Pi$ state of the ion with $n=7$ and $v=1$. It is interesting that also near 0.072 eV, a new final DR channel becomes energetically accessible $[H(n=2)+F(^2P_{1/2})]$, which may help rationalize the fact that after a minimum at about 0.07 eV, DR rebounds to a higher value while RIP continues downward. We offer no specific interpretation nor assignment to the broad peak that DR and RIP both exhibit between 0.002 and 0.02 eV, but point it out as evidence of *indirect* capture.

2. Thermal rate coefficient

For many applications it is useful to have collision data in the form of thermal rate coefficients. At a given temperature T_e, these are evaluated by integrating the product of the cross section and velocity over a Maxwellian velocity distribution. The results for DR and RIP, for electron temperatures ranging from 10 to 1000 K, are shown in Fig. 6. At room temperature, thermal rate coefficients for DR and RIP are 1.96×10^{-8} and 4.53×10^{-9} cm^3 s^{-1}, respectively. Emphasizing again the likely role of indirect capture in the DR for HF^+, the rate coefficient for DR at room temperature is about an order of magnitude lower than that for common diatomic ions. For NO^+ [33], CN^+ [34], CO^+ [35], and

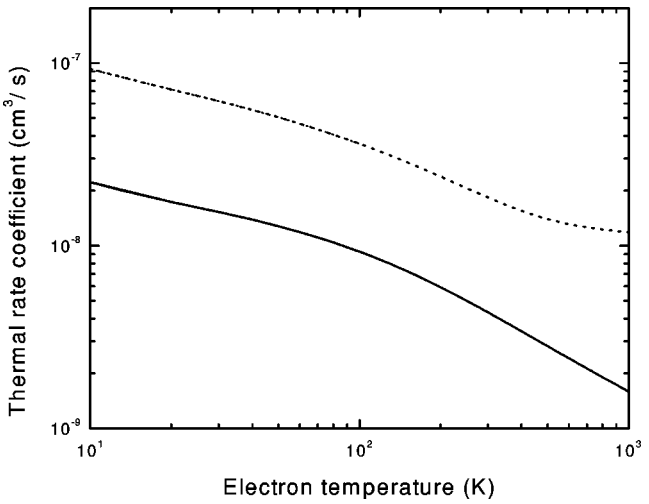

FIG. 6. Thermal rate coefficient of HF^+ ($v=0$) as a function of the electron temperature: dotted line, DR and solid line, RIP.

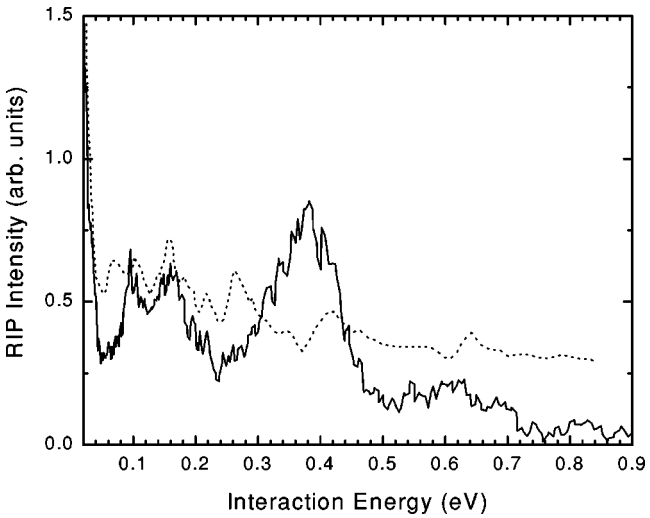

FIG. 7. Comparison of RIP and photo-RIP results. Solid line, product of the RIP cross section (from Fig. 5) multiplied by the c.m. energy plotted as a function of c.m. energy. Dotted curve is taken from the photo-RIP data for HF [23] after subtracting the ionization energy (16.046 eV) to put the two curves on the same energy scale.

N_2^+ [36] the rate coefficients are 4×10^{-7}, 3.4×10^{-7}, 2.75×10^{-7}, and 1.75×10^{-7} $cm^3\,s^{-1}$, respectively. The DR processes for all of these ions are found to be predominantly controlled by a direct mechanism, which involves curve crossing between the ground ionic and doubly excited dissociative neutral-state potential curves. It is worthwhile mentioning other cases where the DR thermal rates of the order of 10^{-8} $cm^3\,s^{-1}$ are obtained. Namely, for HeH^+ [24] HD^+ [37], and OH^+ [38] where different indirect mechanisms are used to explain the DR processes, thermal rates of about 3×10^{-8} $cm^3\,s^{-1}$, 6.9×10^{-9} $cm^3\,s^{-1}$, and 6.3×10^{-9} $cm^3\,s^{-1}$, respectively, were found.

3. Resonant ion-pair production

The additional structural features seen in the RIP cross section, not seen in the DR curves, invite further comment and interpretation. Again, it is useful that important experiments [22,23] with photons have preceded this work, and the associated interpretations can be partly adopted. In the work mentioned, ion-pair formation (we refer to this as photo-RIP) was studied by photoionization of both neutral HF and DF, and by recording the $H^+(+F^-)$ formation from HF and the $D^+(+F^-)$ formation from DF.

For purposes of comparison, the photo-RIP data of Yencha *et al.* [23] (the two sets of data referred to are very similar) are plotted in Fig. 7 on the present energy scale by subtracting the ionization potential of HF (=16.046 eV) [39] from the photon energy. This figure also shows our RIP cross section multiplied by the c.m. energy. The product σE removes the E^{-1} behavior from our experimental data and allows the use of a linear scale. Related features are observed in comparing these two sets of results, especially the peaks at about 0.1 eV and 0.15 eV. However, relative strengths and exact locations of various peaks differ between the two processes. For example, the strong RIP peak near 0.38 eV and the smaller one at 0.6 eV both appear, though very weak, and slightly displaced in the photo-RIP spectra.

A summary of peaks seen in the experiments and the assignments given by the authors of photo-RIP are shown in Table I. Also included in Table I are autoinization peak po-

TABLE I. Column 1, selected peak-energy positions for F^- formation from photo-RIP of HF and column 2, their possible Rydberg state assignments taken from [23]; column 3, peak-energy positions for F^- formation from RIP of HF^+; column 4, selected vibrationally autoionized Rydberg levels in HF converging to the $X\,^2\Pi$ state, and their n and v assignments (column 5 and 6) [32].

photo-RIP peak (eV) [23]	Rydberg state assignment	RIP peak (eV)	Autoionization peak (eV) [32]	n	v
0.024	$(A^2\Sigma^+ \quad v=17)\ 3s\sigma$	0.02	0.012	6	1
0.078	$(X^2\Pi_{3/2} \quad v=1)\ 7d$	0.07 minimum	0.073	7	1
0.111	$(X^2\Pi_{1/2} \quad v=1)\ 7d$	0.09	0.091	7	1
0.151 0.174	$(X^2\Pi_{3/2} \quad v=1)\ 8d$	0.14	0.14	8	1
0.2	$(X^2\Pi_{1/2} \quad v=1)\ 8d$	0.2 shoulder	0.182	8	1
0.42	$(A^2\Sigma^+,v)3p\sigma$	0.36-0.42	0.457	7	2
0.583	$(A^2\Sigma^+,v)3p\sigma$	0.6			

sitions observed in photoionization studies of HF and Rydberg states (converging to the $v=1$ and $v=2$ levels of the $X\,^2\Pi$ state) assignments as originally proposed by Berkowitz *et al.* [22] and later assigned by Guyon *et al.* [32].

Interpretations given by both Berkowitz *et al.* and Yencha *et al.* [22,23] say that photo-RIP of HF does not proceed through direct excitation to the repulsive $V\,^1\Sigma^+$ ion-pair state, but rather by predissociation of bound Rydberg states. Berkowitz *et al.* [22] explained the involvement of intermediate Rydberg states that predissociate via the $V\,^1\Sigma^+$ ion-pair state rather than via direct transition from the ground state of HF to the $V\,^1\Sigma^+$ state by the fact that the observed width of the first photo-RIP peak is too small to correspond to the Franck-Condon overlap [see the Franck-Condon region shown between the vertical lines in Fig. 1(a)] between the ground HF state and the repulsive part of the excited $V\,^1\Sigma^+$ state [22]. Both groups of authors [22,23] find the first peak maximum at 16.070 eV ($16.070-16.046=0.024$ eV on our scale) for F^- formation, which agrees well with the position of the maximum at 0.02 eV observed in our RIP data. In the paper of Yencha *et al.* [23], this first strong peak was assigned to high vibrational levels ($v=17,18$) of the core-excited $3s\sigma$ Rydberg state converging to the $A\,^2\Sigma^+$ ion-excited state [Fig. 1(a)]. Most of the structure immediately following the first peak is explained by both groups of authors [22,23] to be photoexcitation to the Rydberg states that converge to the $v=1$ and $v=2$ levels of both components of the $X\,^2\Pi$ ground state. As shown in Table I, some peaks are assigned by Yencha *et al.* [23] to be due to vibrational levels of the second Rydberg state, the $3p\sigma$ state, also converging to the $A\,^2\Sigma^+$ ion-excited state. Clearly, the energy positions of all of the Rydberg peaks shown in Fig. 7 are not given in Table I.

Although the match between the results shown in Fig. 7 is not perfect, there is a correspondence between them. The disparity between RIP and photo-RIP intensities of the peaks at 0.4 eV and 0.6 eV has already been referred to. This discrepancy is one indication that the electron-capture process can access states that are forbidden by radiative transitions. Thus, when comparing our RIP results with the photodissociation data, one has to keep in mind a few differences between these two experimental approaches. In our experiment the transitions are neither controlled nor driven by optical selection rules. Another difference is that the equilibrium internuclear separations are different for HF ($R_e=0.1001$ nm) and HF^+ ($R_e=0.1224$ nm), and consequently Franck-Condon regions that control the transitions are different.

IV. SUMMARY

The results on HF^+ reported here represent the first measurements of rates and cross sections for DR and RIP of a halogen halide ion. We have obtained DR rates significantly smaller than those for common diatomic molecular ions despite the crossing of the ionic $V\,^1\Sigma^+$ potential curve with the ground-state ion between the classical turning points of the $v=0$ vibrational level. This fact and the presence of structure in the cross section that generally decreases as E^{-1} led us to conclude that the electron capture takes place both by the normal direct process and by indirect processes that interfere. Also, contrary to the other few cases that have been investigated, resonant ion-pair formation competes strongly with DR, accounting for about 25% of the total ''recombinations'' at low energies. A strong complementarity has been found between RIP in HF^+ and the process of ion-pair production by photodissociation of HF, a process we have called photo-RIP. The interpretation of the photo-RIP data have been adopted in discussing many of the structures found in the RIP cross section.

The interesting energetics of HF and HF^+ and the availability of a significant amount of data on the systems should make DR and RIP likely candidates for theoretical investigation.

ACKNOWLEDGMENTS

This work was supported in part by the Office of Fusion Energy of the U.S. Department of Energy under Contract No. DE-A102-95ER54293 with the National Institute of Standards and Technology. This work was also supported by the Swedish Natural Science Research Council, the Göran Gustafson Foundation for Research in Natural Science and Medicine, and the Swedish Foundation for International Cooperation in Research and Higher Education.

[1] M. Larsson, Adv. Ser. Phys. Chem. **10**, 693 (2000).

[2] S. L. Guberman, in *Dissociative Recombination: Theory, Experiment and Applications*, edited by J. B. A. Mitchell and S. L. Guberman (World Scientific, Singapore, 1989) p. 45.

[3] Z. Amitay, D. Zajfman, P. Forck, U. Hechtfischer, B. Seidel, M. Grieser, D. Habs, R. Repnow, D. Schwalm, and A. Wolf, Phys. Rev. A **54**, 4032 (1996).

[4] Z. Amitay, D. Zajfman, P. Forck, T. Heupel, M. Grieser, D. Habs, D. Schwalm, A. Wolf, and S.L. Guberman, Phys. Rev. A **53**, R644 (1996).

[5] L. Carata, A.E. Orel, M. Raoult, I.F. Schneider, and A. Suzor-Weiner, Phys. Rev. A **62**, 052711 (2000).

[6] See, for example, *Dissociative Recombination: Theory, Experiment and Applications IV*, edited by M. Larsson, J. B. A. Mitchell, and I. F. Schneider (World Scientific, Singapore, 2000); *Dissociative Recombination: Theory, Experiment and Applications III*, edited by D. Zajfman, J. B. A. Mitchell, D. Schwalm, and B .R. Rowe, (World Scientific, Singapore, 1996); M. Larsson, Annu. Rev. Phys. Chem. **48**, 151 (1997).

[7] G. H. Dunn and N. Djurić, in *Novel Aspects of Electron-Molecule Scattering*, edited by K. Becker (World Scientific, Singapore, 1998), pp. 241–281.

[8] B. Peart and K.T. Dolder, J. Phys. B **8**, 1570 (1975).

[9] B. Peart, R.A. Forest, and K.T. Dolder, J. Phys. B **12**, 3441 (1979).

[10] F.B. Yousif, P. Van der Donk, and J.B. Mitchell, J. Phys. B **26**, 4249 (1993).

[11] G.V. Dubrovski and V.D. Ob'edkov, Theor. Exp. Chem. **2**, 715 (1966); Vth International Conference on Physics of Electronic and Atomic Collisions, Leningrad, 1965, Abstracts of papers, p. 342.
[12] Å. Larson and A.E. Orel, Phys. Rev. A **59**, 3601 (1999).
[13] W. Zong, G.H. Dunn, N. Djurić, M. Larsson, C.H. Green, A. Al Khalili, A. Neau, A.M. Derkatch, L. Vikor, W. Chi, A. Le Padellec, S. Rosén, H. Danared, and M. af Ugglas, Phys. Rev. Lett. **83**, 951 (1999).
[14] Å. Larson, N. Djurić, W. Zong, C.H. Green, A.E. Orel, A. Al Khalili, A.M. Derkatch, A. Le Padellec, A. Neau, S. Rosén, W. Shi, L. Vikor, H. Danared, M. af Ugglas, M. Larsson, and G.H. Dunn, Phys. Rev. A **62**, 042707 (2000).
[15] *The 118 reported interstellar and circumstellar molecules*, compiled by the National Radio Astronomy Observatory 1997. http://www.cv.nrao.edu/~awootten/allmols.html
[16] http://www.nap.edu/readingroom/books/planet_sci/contents/chap4b.html
[17] http://members.aol.com/magnu96196/hf.html
[18] T. Hoshino and Y. Nishioka, J. Chem. Phys. **111**, 2109 (1999).
[19] http://xxx.lanl.gov/abs/astro-ph/9708013
[20] A.J. Yencha, A.J. Cormack, R.J. Donovan, A. Hopkins, and G.C. King, J. Chem. Phys. **32**, 2539 (1999).
[21] *NIST Chemistry WebBook*, NIST Standard Reference Database Number 69, edited by. W.G. Mallard and P.J. Linstrom, (National Institute of Standards and Technology, Gaithersburg MD, 2000 (http://webbook.nist.gov).
[22] J. Berkowitz, W.A. Chupka, P.M. Guyon, J.H. Holloway, and R. Spohr, J. Chem. Phys. **54**, 5165 (1973).
[23] A. Yencha, A. Hopkirk, J.B. Grover, B.-M. Cheng, H. Lefebvre-Brion, and F. Keller, J. Chem. Phys. **103**, 2882 (1995).
[24] C. Strömholm, J. Semaniak, S. Rosén, H. Danared, S. Datz, W. van der Zande, and M. Larsson, Phys. Rev. A **54**, 3086 (1996).
[25] H.J. Werner, P. Rosmus, W. Schätzl, and W. Meyer, J. Chem. Phys. **80**, 831 (1984).
[26] H. Danared, Nucl. Instrum. Methods Phys. Res. B **79**, 269 (1993).
[27] H. Danared, G. Andler, L. Bagge, C.J. Herrlander, J. Hilke, J. Jeansson, A. Källberg, A. Nilsson, A. Paál, K.-G. Rensfelt, U. Rosengård, J. Starker, and M. af Ugglas, Phys. Rev. Lett. **72**, 3775 (1994).
[28] J.R. Mowat, H. Danared, G. Sundström, M. Carlson, L.H. Andersen, L. Vejby-Christensen, M. af Ugglas, and M. Larsson, Phys. Rev. Lett. **74**, 50 (1995).
[29] D. Kilgus, D. Habs, D. Schwalm, A. Wolf, N.R. Badnell, and A. Müller, Phys. Rev. A **46**, 5730 (1992).
[30] A. Lampert, A. Wolf, D. Habs, J. Kenntner, G. Kilgus, D. Schwalm, M.S. Pindzola, and N.R. Badnell, Phys. Rev. A **53**, 1413 (1996).
[31] D.R. DeWitt, R. Schuch, T. Quinteros, H. Gao, W. Zong, H. Danared, M. Pajek, and N.R. Badnell, Phys. Rev. A **50**, 1257 (1994).
[32] P.M. Guyon, R. Spohr, W.A. Chupka, and J. Berkowitz, J. Chem. Phys. **65**, 1650 (1976).
[33] L. Vejby-Christensen, D. Kella, H.B. Pedersen, and L.H. Andersen, Phys. Rev. A **57**, 3627 (1998).
[34] A. Le Padellec, J.B.A. Mitchell, A. Al-Khalili, H. Danared, A. Källberg, Å. Larson, S. Rosén, M. af Ugglas, L. Vikor, and M. Larsson, J. Chem. Phys. **110**, 890 (1999).
[35] S. Rosén, R. Peverall, M. Larsson, A. Le Padellec, J. Semaniak, Å. Larson, C. Strömholm, W.J. van der Zande, H. Danared, and G.H. Dunn, Phys. Rev. A **57**, 4462 (1998).
[36] J.R. Peterson, H. Danared, G.H. Dunn, M. Larsson, A. Le Padellec, Å. Larson, R. Peverall, C. Strömholm, S. Rosén, M. af Ugglas, and W.J. van der Zande, J. Chem. Phys. **108**, 1978 (1998).
[37] A. Al-Khalili, Ph.D. thesis, Stockholm University, Sweden, 2000.
[38] S.L. Guberman, J. Chem. Phys. **102**, 1699 (1995).
[39] A. Mank, D. Rodgers, and J.W. Hepburn, Chem. Phys. Lett. **229**, 169 (1994).